NUMERICAL INVESTIGATION OF FLOW DISTRIBUTIONS IN LIQUID FUEL MOLTEN SALT REACTORS

A Thesis

by

MICHAEL S. LEWANDOWSKI

Submitted to the Graduate and Professional School of
Texas A&M University
in partial fulfillment of the requirements for the degree of

MASTER OF SCIENCE

Chair of Committee,	Mark Kimber
Committee Members,	Pavel Tsvetkov
	Nagamangala Anand
Head of Department,	Michael Nastasi

May 2023

Major Subject: Nuclear Engineering

ABSTRACT

A computational fluid dynamics investigation was conducted to evaluate the thermal-hydraulic behavior within a molten salt nuclear core for a given heat generation profile. The entry length behavior, maximum temperature, and radial temperature gradient are investigated to provide insight as to the effective heat removal capabilities for two domains. The first flow geometry evaluated was a fully developed, 1D laminar flow in a cylindrical flow channel within a hexagonal graphite unit cell with internal heat generation in both the fluid and solid domains. This flow geometry had adiabatic boundary conditions imposed upon the outer wall of the graphite, and entry length behavior of the fluid was investigated to provide insight to the value of the effective heat transfer coefficient for a given coolant channel within a molten salt reactor core, as well as characterizing it as a function of height. An array of the hexagonal unit cell organized into a 60-degree wedge which represent a simplified molten salt reactor core region was next evaluated. The aim of this evaluation was that for a given heat generation profile, which was axially and radially dependent, by controlling the mass flow rate through each channel the radial temperature gradient and maximum temperature can be minimized, thus minimizing the thermal stresses. This minimization of the radial temperature gradient is also beneficial for neutronic evaluation, as the radial density distribution of the fuel salt is temperature dependent. Furthermore, the minimization of the maximum temperature in the reactor core is desired for both structural and neutronic purposes, as a significantly large thermal maximum could induce structural failure or a local perturbation of the neutron flux in that region due to temperature feedback effects and local density variation. It was found that due to the internal heat generation in the solid graphite domain, the maximum temperature was located in the graphite and the fuel salt acted as a coolant, rather than depositing heat into the graphite. The ideal mass flow rate distribution was found, and the

combined entry length behavior of a channel in that case was evaluated. Application of this methodology provides key insight into the design specifications needed for a flow distributor which could be present in the lower plenum region.

DEDICATION

To my parents, who have unconditionally loved and supported me.

To my sisters, who have shown me what it means to be successful in life.

To my friends, who have made life great.

ACKNOWLEDGEMENTS

The author would like to thank Dr. Mark Kimber, for his endless patience and support as both a professor and a friend.

The author would also like to thank Dr. Paul Kristo, who went above and beyond as a mentor and taught invaluable skills and knowledge. Without his guidance and teachings this work would not have come to fruition.

CONTRIBUTORS AND FUNDING SOURCES

Contributors

This work was supervised by a thesis committee consisting of Dr. Mark Kimber and Dr. Pavel Tsvetkov of the Department of Nuclear Engineering, and Dr. N.K. Anand of the Department of Mechanical Engineering.

Funding Sources

Graduate study was supported by the Department of Nuclear Engineering at Texas A&M and the Nuclear Energy eXperimental Lab Research Alliance (NEXTRA).

TABLE OF CONTENTS

Page

LIST OF FIGURES

Page

LIST OF TABLES

Page

LIST OF EQUATIONS

Page

INTRODUCTION

A nuclear reactor core generates heat through fission reactions, where a neutron impacts the nucleus of a fissile material and induces a fission reaction. This reaction releases mass and energy, where the energy is primarily in the form of heat in the fissile material, which can be used in power plants to generate electricity. Within the nuclear industry, both international and domestic, there is a push to develop new reactor technologies and build next generation reactors, as they are hypothesized to be significantly safer and more economically viable. This effort can be formally recognized as the internationally sanctioned Generation-IV Forum (GIF), which at its inception was an agreement between 9 countries (approximately 40 countries are participants to date) to co-operatively develop the research and technology of fourth-generation nuclear systems and make them available for industrial deployment by 2030 [1]. The generation 4 reactor type being evaluated as part of this investigation was the liquid fuel molten salt reactor. In liquid fuel molten salt reactors, the fissile material (typically Uranium-235) is dissolved into the molten salt coolant and pumped through a closed loop system to generate power. Within the closed-loop system the fissile fuel salt will flow through the reactor core, where graphite will provide local moderation to the system and allow for a nuclear chain reaction to occur. If the flow distribution within the core is properly designed, the fuel salt will ultimately move away from the core region and flow around the loop, and as it does so it moves away from the graphite moderator and exits the region where a nuclear chain reaction is possible. This has numerous safety advantages, but a key advantage of the design is that the majority of the heat generation is within the coolant. Whereas a conventional light water nuclear reactor design has non-negligible thermal resistance between the heat generation location and the coolant leading to large thermal gradients within the core, a molten

salt reactor predominantly generates the heat within the coolant. The reduction of the magnitude of thermal gradients within the core is desired from a mechanical and structural design stance, as strong local thermal gradients indicate an associated thermal stress in that location [2]. Furthermore, large temperature gradients complicate neutronic calculations due to significantly varied cross-sections, introducing feedback effects of differing magnitude, and non-negligible spatial density variation. The aim of this investigation is to provide the ideal flow distribution based upon a core geometry and associated heat generation profile, as well as a simplified equation which can give an approximate flow distribution based upon the heat generation profile.

In typical power generating nuclear reactors, the bulk flow of the coolant is flowed across the highest power density region, which is typically the fuel located at the geometric center of the active core [3]. This is due to the fuel that undergoes the maximum power generation must receive more coolant to ensure that it remains under the maximum thermal limit allowed by the operating license [4]. To properly compare a conventional solid-fuel reactor to a liquid-fuel reactor, the concept of residence time must be considered. In a conventional power reactor, all of the fuel, structural materials, and graphite moderators will be in the core the entirety of operation, and at no point should exit the active core region, and as such have infinite residence time. In a molten salt liquid-fuel reactor the fuel has a finite residence time in the active core region, whereas the structural materials and the graphite have infinite residence time. The fuel undergoes fission reactions, and as such have the highest magnitude heat generation profile. However, because the fuel exits the core and the graphite remains in the active core region, despite experiencing a significantly lower magnitude of heat generation the graphite in steady state must be cooled or will exceed the thermal limitation before the fuel. The aim of this thesis was to identify the ideal mass flow distribution to minimize the maximum temperature and minimize the radial temperature

gradient in the core, as well as the investigation of the combined entry length problem under the thermal conditions that occur within a molten salt reactor. This mass flow distribution will be dependent upon the heat generation profiles in both fuel salt and graphite, the geometry of the fuel channels and graphite blocks, as well as the boundary conditions imposed upon the overall domain.

Previous Molten Salt Reactors

While molten salt nuclear reactors are considered as part of advanced nuclear reactor technology, the concept and physics of a molten salt reactor are over seventy years old [4]. The first investigation of molten salt reactors started in the 1940's as part of a United States program to develop a nuclear-powered plane, and in 1954 the Aircraft Reactor Experiment (ARE) operated successfully for 9 days without any mechanical or chemical problems occurring. This led to Oak Ridge National Labs constructing and operating the Molten-Salt Reactor Experiment (MSRE), which was an 8 MW thermal reactor, with a fluoride fuel salt moderated by graphite within the core [6]. The MSRE first went critical on June 1, 1965, and operated in low power ranges while calibrating all operating equipment. In January of 1966 the reactor began its climb to full power, and within hours problems in the off-gas system resulting in a shutdown of the reactor while safety inspections occurred. After this problem was resolved through the installation of a more efficient filtering system, a second attempt to reach full power began. As the reactor neared full power, it was discovered that the heat removal capability of the secondary heat-exchanger had been overestimated due to the thermophysical properties of the coolant salt not being accurately understood, and as such the reactor was restricted to 8 MW as the new full power mark. Operation of the MSRE from this point onwards roughly followed the pre-determined operating schedule, however due to operating or mechanical failures there were unscheduled periods of time where the

reactor was shut down for maintenance. Ultimately the operation of the MSRE demonstrated that the physics of a molten salt reactor is sound, and provided valuable information towards fuel chemistry, chemical processing of fuel salt, material compatibility in a molten salt reactor, and reactor dynamics [7].

As the nuclear industry expands into Generation-IV reactor technologies, molten salt reactors are being designed and undergoing the licensing process in the United States. The Nuclear Energy eXperimental Testing (NEXT) Lab in Abilene, Texas has set out to design, license, and commission a molten salt research reactor [8]. NEXT Lab has partnered with Texas A&M, The University of Texas, and Georgia Institute of Technology under the research consortium NEXT Research Alliance (NEXTRA) to fulfil the goal of commissioning a molten salt reactor. It is in support of this goal that this investigation into the ideal flow distribution through a molten salt reactor core was carried out, as well as investigating the entry-length behavior of the fuel salt as it both hydro-dynamically and thermally develops through the active core region.

Entry Length Phenomena

When determining a molten salt nuclear core coolant distribution, or any heat removal apparatus, the effective heat transfer coefficient for each coolant path is needed to accurately assess the effective heat removal rate for a given channel as well as overall performance. While there are known solutions to the thermally fully developed region [2], in the entry region the solution to the energy equation becomes significantly more difficult to obtain, as both velocity and temperature depend upon the bulk direction of the flow as well as the radial direction. Within a reactor core once the flow enters a coolant channel it develops both hydrodynamically as well as thermally, leading to what is known as the combined entry length problem. Kays et al. [9] investigated two

thermal boundary conditions upon the fluid wall, being constant heat flux and constant temperature, and provided solutions to both combined entry length conditions. Their investigation found that the Nusselt number is effectively infinite at the initialization of the flow and decayed down to a converged value of 4.36 or 3.66, for the constant heat flux and constant temperature boundary conditions respectively. However, neither of those boundary conditions are applicable in a reactor core coolant channel. As the coolant progress along the channel, the channel walls temperature will vary as a function of height and radial position due to the non-homogeneous power generation profile within the reactor core. In addition to the boundary conditions not being suitable, there is internal heat generation within the fuel salt coolant in liquid fuel molten salt reactors, something which was not considered in the solution provided by Kays. For this reason, the Nusselt number, and by extension the effective heat transfer coefficient, were evaluated as a function of reactor height.

METHODOLOGY

To properly investigate the desired phenomena, the ANSYS software suite was chosen as it provided both robust tools suited to this investigation, as well as ample documentation on both proper operation of each software package, as well as the mathematics applied during simulation. ANSYS SpaceClaim was used to construct the geometries, Mechanical Meshing was utilized to mesh the fluid and solid domains, and Fluent was used as the computational fluid dynamics (CFD) tool to simulate the thermal-hydraulic phenomena. While other validated software could undoubtedly be used and arrive at similar results, ANSYS was chosen for the above reasons, and that it was designed as an interconnected software suite which streamlined the workflow.

Geometry

Two geometries were constructed in ANSYS SpaceClaim to be used in this investigation, the first was a solid hexagonal unit cell with a cylindrical flow domain centered inside the solid, and the second was an array of the hexagonal unit cells organized into a 60-degree wedge to represent a simplified active core region domain. The hexagonal unit cell is shown in Figure 1, and the core geometry is depicted in Figure 2. Both geometries were oriented such that the fluid flows along the +y-axis, with the origin for the unit cell being the precise center of the inlet face and the origin of the core wedge being the point of the slice which represents the geometrical center of the reactor core. For both geometries the fuel salt was represented as the red region, and the graphite as green.

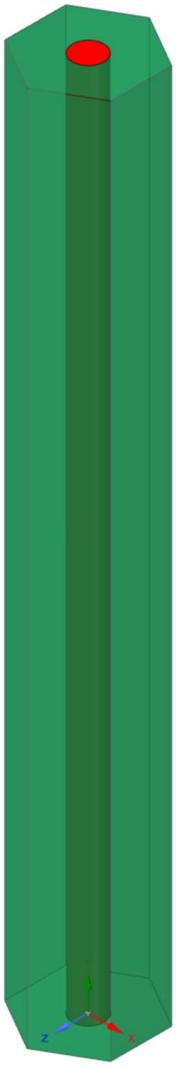

Figure 1: Hexagonal Unit Cell

The fuel channel had a diameter of 30.16 mm (1.19 inch), the hexagonal blocks had a pitch of 101.6 mm (4 inch), and the entire unit cell had an axial height of 800 mm (31.50 inch). The fuel channel had a total volume of 571534.3703 mm^3 (34.8771 in^3), and the graphite had a total volume of 6580138.9894 mm^3 (401.5447 in^3).

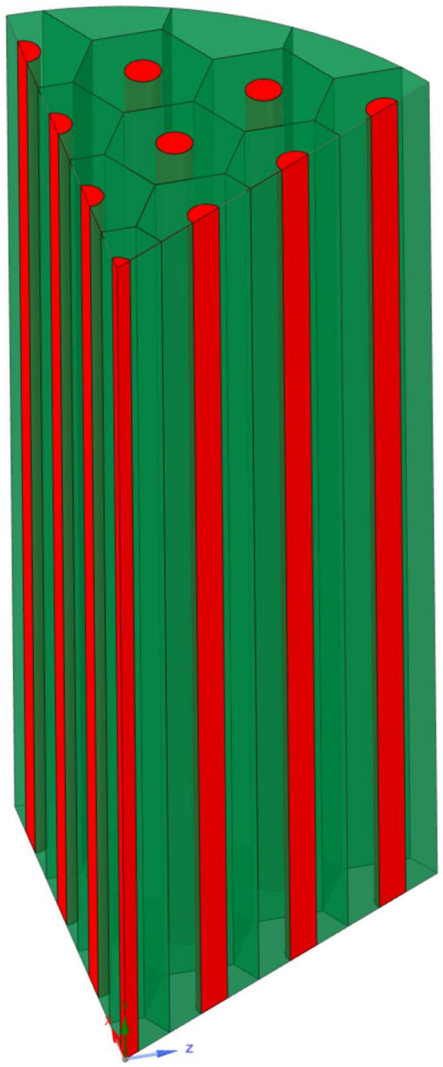

Figure 2: Core Wedge

The core wedge geometry was constructed by placing multiple hexagonal unit cells adjacent to one another until a wedge with 4 channels in the radial direction had been generated. Next two slicing planes were generated, one as the xy-plane and the second as an xy-plane that was rotated 60-degees towards the z-axis. Any geometry that penetrated these planes was cut away, leaving a 60-degree domain. Next the “sweep arc” function was utilized to appropriately apply an

arc at the circumference of the wedge. Any fuel salt channels that would have been split by the arc were filled in with graphite. The total graphite volume in the core wedge domain was 49443510.6068 mm^3 (3017.2281 in^3), and the total fuel salt volume was 3524463.7581 mm^3 (205.0760 in^3). This wedge contains one $1/6^{th}$ channel, six 1/2 channels, and 3 full channels.

Mesh Generation

In order to utilize CFD in the computational domain to obtain valid results, the domain must be discretized into differential volumes where governing differential equations can be solved. This was done in ANSYS Mechanical Meshing, as it is a part of the ANSYS suite and allowed the investigator to specify numerous mesh generation controls [10]. For the hexagonal unit cell, the fluid domain was meshed with tetrahedral nodes, sweeping from a mapped inlet face to the outlet. The graphite domain was also meshed with tetrahedral nodes, sweeping from the bottom of the domain (y = 0.00 mm or 0.00 in) to the top of the domain (y = 800.00 mm or 31.496 in). A maximum size restriction of 2.5 mm (0.984 in) was imposed upon the fluid domain, and a size restriction of 5 mm (0.197 in) was imposed upon the solid domain. The combined fluid and solid mesh had a maximum aspect ratio of 4.867, and a minimum orthogonal quality of 0.573. For the core wedge meshing controls, a tetrahedral mesh was generated, sweeping from each inlet (which was designated as a mapped mesh face) to its associated outlet. A sizing restriction of 2.5 mm (0.984 in) was implemented throughout the fluid domain. The graphite domain had a sizing restriction of 5 mm (0.197 in). The combined fluid and solid mesh had a maximum aspect ratio of 6.156, and a minimum orthogonal quality of 0.423. Evaluation of mesh independence for both the hexagonal unit cell and the core wedge meshes are presented in a later section.

Simulation

As part of the ANSYS software suite, Fluent is provided as one of several CFD packages. Fluent was used over CFX or Polyflow (other ANSYS CFD packages) because the abundance of documentation and support for Fluent are not present in the other choices. Furthermore, internal heat generation as a function of position is something that can be done in Fluent through the application of a user-defined function. Whereas in CFX and Polyflow implementation of a source term such as this is considerably more difficult.

Fluent Controls

All cases were run utilizing the laminar viscous model, which was shown to be the correct viscous model in the below section regarding mass flow rate. Every case was run in steady-state, with pressure-based solvers and absolute velocity formulation. For all cases gravity effects were disabled ensure the thermal-hydraulic effects can be isolated and investigated. The pressure-velocity coupling utilized a coupled scheme as opposed to a segregated solution scheme. The spatial discretization schemes were as follows; least squares cell based for gradient, second order for pressure, and second order upwind for momentum and energy. The pseudo-transient explicit relaxation factors for pressure and momentum were 0.5, for energy 0.75, and 1.0 for density and body forces. Convergence criteria of $1x10^{-4}$ for continuity, x-,y-,z-velocity equations, and $1x10^{-6}$ for energy were implemented.

Material Properties

To properly simulate a liquid fuel molten salt reactor, appropriate thermophysical properties must be implemented into the solver or the results are inconsequential. For the molten salt thermophysical properties, of the literature that had been published to date there was a wide range for property values which highly depended upon the amount and type of fissile material dissolved within the salt [11]. However, non-nuclear molten salts had good agreement between various publications [11] and [12]. To ensure that the results of this investigation provide meaningful impact, it was decided that non-nuclear fuel salt, specifically FLiBe would be applied, as this is a widely used solvent for fissile material in molten salt reactors. Nuclear grade graphite material properties from Idaho National Labs (INL) were implemented [14]. These thermophysical properties are presented in Table 1 below.

Table 1: Thermophysical Properties

Material	Density [kg m^{-3}]	Specific Heat [j kg^{-1} K^{-1}]	Thermal Conductivity [W m^{-1} K^{-1}]	Viscosity [kg m^{-1} s^{-1}]
FLiBe	1940	2414.17	1	0.0056
Graphite	1870.5	1697.43	82.22	N/A

Density

Density was considered a constant value throughout all simulations, for both the liquid salt and the solid nuclear grade graphite. This was done for two primary reasons, firstly that the data for the molten salt used was of non-nuclear liquid salt, that is that the properties that of FLiBe salt without Uranium dissolved within, and there was insufficient data on the density of the nuclear

FLiBe salt when this investigation began. The second reason was that the domain and mesh were not set up to handle the thermal expansion in the solid graphite region to maintain a mass balance within the core. In order to handle a dynamic solid domain throughout a simulation, significantly more computational resources are required to accurately simulate and reach convergence [14]. If sufficient data was readily available, the density of the fuel salt would have been set to be a function of temperature which would impact the results.

Boundary Conditions

To best simulate a reactor core, while being cognizant of computational resources and maintaining the ability to apply the results to future work, the following thermal boundary conditions were applied to the domain. The bottom of the computational domain, where the inlets to the fuel channels are located, are set to a constant temperature of 500 Kelvin for both the fuel salt and the graphite. The external and top walls of the graphite were set to adiabatic thermal conditions. The fluid to solid interface was set as no-slip for the hydraulic interface condition and internal coupled wall for the thermal condition. In Fluent, an internal coupled wall boundary condition allows for all three mechanisms of heat transfer (conduction, convection, and radiation), and calculates the effective heat transfer across the interface based upon the material properties and thermal-hydraulic phenomena occurring about a given interface. The emissivity at the wall was set to zero to eliminate any radiative heat transfer across the boundary. By choosing this interface condition, the solver can properly assess the thermal-hydraulic phenomena that is being investigated. The fluid inlet conditions are velocity inlet conditions, where a uniform velocity is imposed across the entire area of the inlet for the array of channels. In the single unit cell case, a user-defined function (UDF) was imposed to give the inlet velocity profile that of a fully developed

laminar flow profile. Where the domain was split into the $1/6^{th}$ slice, symmetry boundary conditions were imposed which allows for a reduction in computational resources upon the assumption that the core behavior is axisymmetric. This is a reasonable assumption as reactor power and heat generation profiles exhibit this behavior [16].

Mass Flow Rate

Various reactor designs undoubtedly exhibit various mass flow rates, specifically power generation reactors will have the mass flow rate magnitude tuned to the desired electrical power rate [15]. For this investigation a total primary loop mass flow rate of 10 kg s^{-1} was selected, as this forced all selected mass flow rates through each channel to be laminar, which occurs when the Reynolds number is less than 2000. It should be noted that by forcing laminar flow, a conservative estimate of the heat transfer coefficient is applied as turbulent flow exhibits higher heat transfer coefficients and therefore is more effective at removing thermal energy. The formula for the Reynolds number in a circular cross section is shown in Equation 1, and when the values applied in this investigation are substituted the resultant falls within the laminar regime. As the simplified core model is a $1/6^{th}$ slice of the overall flow domain, the sum of all core channel mass flow rates in the simplified core model must equal 1.6667 kg s^{-1}. For the hexagonal unit cell geometry and all cases run upon it, a mass flow rate of 0.1379 kg s^{-1} was applied, which corresponded to an inlet velocity of 0.1 m s^{-1}.

Equation 1: Reynolds Number Equation

$$Re = \frac{\rho U D}{\mu}$$

Where,

ρ is the fluid density in kg m^{-3}

U is the fluid bulk velocity in m s^{-1}

D is the diameter of the cross-sectional area in m

and μ is the fluid viscosity in kg m^{-1} s^{-1}

Re is the Reynolds number

Heat Generation

In a molten salt nuclear core, all materials undergo some amount of internal heat generation due to radiation effects. The liquid fuel salt will have the highest magnitude of heat generation due to the fissile material dissolved within undergoing nuclear fission, while the other materials will generate heat due to energy deposition by the radiation. To mimic this behavior, internal heat generation was applied to the simulations. For the single fuel channel simulations investigating thermal entry length, a uniform heat generation was imposed upon both the fluid and solid domains, where the magnitude in the fuel salt represented 95 % of the total heat generation and the graphite contained the remaining 5 %. For these simulations the total heat generations was set to 500 Watts. For the core wedge a heat generation profile was imposed that was both radially and axially dependent, utilizing trigonometric functions to represent a centralized heat generation

profile. The total power generation in the core wedge model totaled approximately 42 kW which would raise the average fuel salt temperature by 10 Kelvin in the core as calculated through an energy balance. This profile is shown in Equation 2, and imposed through the use of a user-defined function (UDF) in Fluent. UDFs are written in the C+ language as script files and allow the user to specify field variable values based upon their position, among other things that would not be possible while using the base level of Fluent operating conditions.

Equation 2: Heat Generation Profile

$$q''' = \chi_{s,g} * P_{s,g} * \cos(r * \alpha) * \sin(y * \beta)$$

Where,

$\chi_{s,g}$ is the percentage of total heat generated in the fuel salt or graphite

$P_{s,g}$ is a scaling coefficient based upon the volume of the fuel salt or graphite

α is equivalent to:

$$\alpha = \frac{\pi}{2 * R_{max}}$$

and β is equivalent to:

$$\beta = \frac{\pi}{Y_{max}}$$

Uniformity Index

To evaluate the magnitude of the thermal gradient in the radial direction, a sampling surface was placed in the axial midpoint of the core wedge domain which spanned the radial direction. This sampling surface did not impact the results in any form but allowed for the user to extract and evaluate the field variables in that surface. As part of the built-in capabilities of Fluent, the option to calculate the "Uniformity Index" exists, which represent how a specified field variable varies over a surface [16]. The equation utilized to calculate this metric is shown in Equation 3, for this metric, a value of 1 represents the highest uniformity. This index was used to evaluate the magnitude of thermal gradient, as a high uniformity index would imply that there was minimal variation in the sampling surface.

Equation 3: Uniformity Index

$$y_a = 1 - \frac{\sum_{i=1}^{n}(|\phi_i - \varphi_a)A_i}{2 |\varphi_a \sum_{i=1}^{n} A_i}$$

Where,

i is the facet index of a surface with n facets,

and φ_a is the average value of the field variable over the surface:

$$\varphi_a = \frac{\sum_{i=1}^{n} \phi_i A_i}{\sum_{i=1}^{n} A_i}$$

Mesh Independence Evaluation

To ensure that the meshing controls were adequate a mesh independence evaluation was carried out to ensure that the results from the simulation had minimal discretization error and were independent of mesh refinement. The concept of mesh independence stems from ensuring that when discretizing a domain upon which differential equations will be solved on, one must ensure that the grid is sufficiently refined enough to accurately capture the thermal-hydraulic phenomena that occur. However, an overly refined grid results in an increase in truncation error, which is the result of non-finite numbers, such as pi, being truncated to the precision of the solver and applied hundreds of thousands of times across the solver resulting in inaccurate results. The overall mesh sizing requirement for both meshes were varied by a factor of 0.5x and 2.0x, note that this did not result in an equivalent change in magnitude of nodal positions within the mesh by those factors. The maximum temperature in either solid or fluid domain was used as the value judgement to evaluate the independence, as it is a key parameter in a thermal-hydraulic simulation. For the core wedge domain, the mass flow distribution of Case 4 was applied. The results of this evaluation are shown in Table 2, which clearly showed that the mesh controls were suitable as the maximum temperature had negligible change between refinements.

Table 2: Mesh Independence Evaluation

Domain	0.5x Sizing	1.0x Sizing	2.0x Sizing
Hexagonal Unit Cell	503.242	502.910	503.154
Core Wedge	518.856	519.418	519.197

RESULTS

This section covers the results of the simulations, sectioned by which domain was being investigated. Results for the hexagonal unit cell are presented first, as the findings regarding entry length behavior are applied towards the optimal case of the core wedge and discussed.

Hexagonal Unit Cell

The hexagonal unit cell served two functions in this investigation, firstly it provided a circular flow channel where the validation of the flow physics in Fluent could be carried out. Secondly it allowed for the investigation of the thermal entry length behavior, specifically how the Nusselt number will change as function of position in the presence of internal heat generation in both the fluid and solid domains.

Validation of Fluent

To validate that the results calculated by Fluent are accurate, an isothermal case of fully developed laminar flow in the fuel channel was set-up and executed. This case was chosen as there is an analytical solution for the pressure drop under these conditions. The velocity inlet had a UDF applied which implemented the velocity profile for fully developed laminar flow in the channel (shown in Equation 4). For a fully developed laminar flow, the pressure gradient can be calculated as a function of bulk velocity, viscosity, and radial maximum, which is presented in Equation 5. The converged pressure drop from the Fluent simulation was compared with the analytical solution result

Table **3**, where it can be seen that the results have relatively good agreement, with an overestimation by 8.326 % in the simulation. This percentage was considered to be the relative error for all results in this study.

Equation 4: Laminar Velocity Profile in Round Cross Section

$$\frac{u(r)}{U_m} = 2 * [1 - \left(\frac{r}{r_o}\right)^2]$$

Where,

u(r) is the fluid velocity as a function of radial position in m s^{-1}

U_m is the mean velocity of the flow in m s^{-1}

r is the radial position in m

r_o is the maximum radial distance in m

Equation 5: Pressure Drop of Fully Developed Laminar Flow in Round Cross Section

$$\frac{dP}{dx} = \frac{-8 * U_m * \mu}{r_o^2}$$

Where,

$\frac{dP}{dx}$ is the pressure gradient in Pa m^{-1}

r_o^2 is the maximum radial distance in m

U_m is the mean velocity of the flow in m s^{-1}

μ is the viscosity of the fluid in kg m^{-1} s^{-1}

Table 3: Validation of Laminar Flow Pressure Drop

Method	Pressure Drop [Pa]
Analytical	15.760
Fluent	17.192
Absolute Error	1.431
Relative Error	8.326 %

Combined Entry Length Behavior

After the validation of Fluent was carried out, the entry length behavior of the liquid fuel salt was investigated. The hexagonal unit cell had adiabatic boundary conditions applied upon the top and outer walls of the graphite, while the bottom wall was set to the same temperature as the fluid inlet at 500 K. The fuel salt region contained 95 % of the heat generation, and the graphite

contained the remaining 5 %. To evaluate the combined entry length phenomena, the Nusselt number, which is the ratio of convective to conductive heat transfer at the fluid boundary, was plotted as a function of position or non-dimensional distance along the flow path. The equations used to calculate the Nusselt number as a function of y position are shown below in Equation 6 and Equation 7. The values used in the equations were export from Fluent as ASCII files, and post-processed in MATLAB to yield discrete results and figures.

Equation 6: Newton's Law of Cooling

$$q''(y) = h(y) * [\, T_s(y) - T_b(y) \,]$$

Where,

$q''(y)$ is the average surface heat flux at the fuel salt to graphite interface in W m^{-2} as a function of height

$h(y)$ is the local heat transfer coefficient in W m^{-2} K^{-1} as a function of height

$T_s(y)$ is the average wall surface temperature in K as a function of height

$T_b(y)$ is the average fluid bulk temperature in K as a function of height

Equation 7: Nusselt Number Equation

$$Nu(y) = \frac{h(y) * D}{k}$$

Where,

$Nu(y)$ is the average Nusselt number of the flow as a function of height

$h(y)$ is the local heat transfer coefficient in W m^{-2} K^{-1} as a function of height

D is the fuel channel diameter in m

k is the thermal conductivity of the fuel salt, in W m^{-1} K^{-1}

The values for the average surface heat flux, the wall surface temperature, and the fluid bulk temperature as a function of y position are plotted in Figure 3 and Figure 4. As expected both the wall surface temperature and fluid bulk temperature increase as a function of height, however the wall heat flux appears to behave parabolically, exhibiting a maximum at the middle of the domain and local minimums at the beginning and end of the flow domain. These figures clearly illustrated that the thermal-hydraulic boundary conditions in a molten salt reactor coolant channel cannot be assumed as either constant heat flux or constant wall temperature.

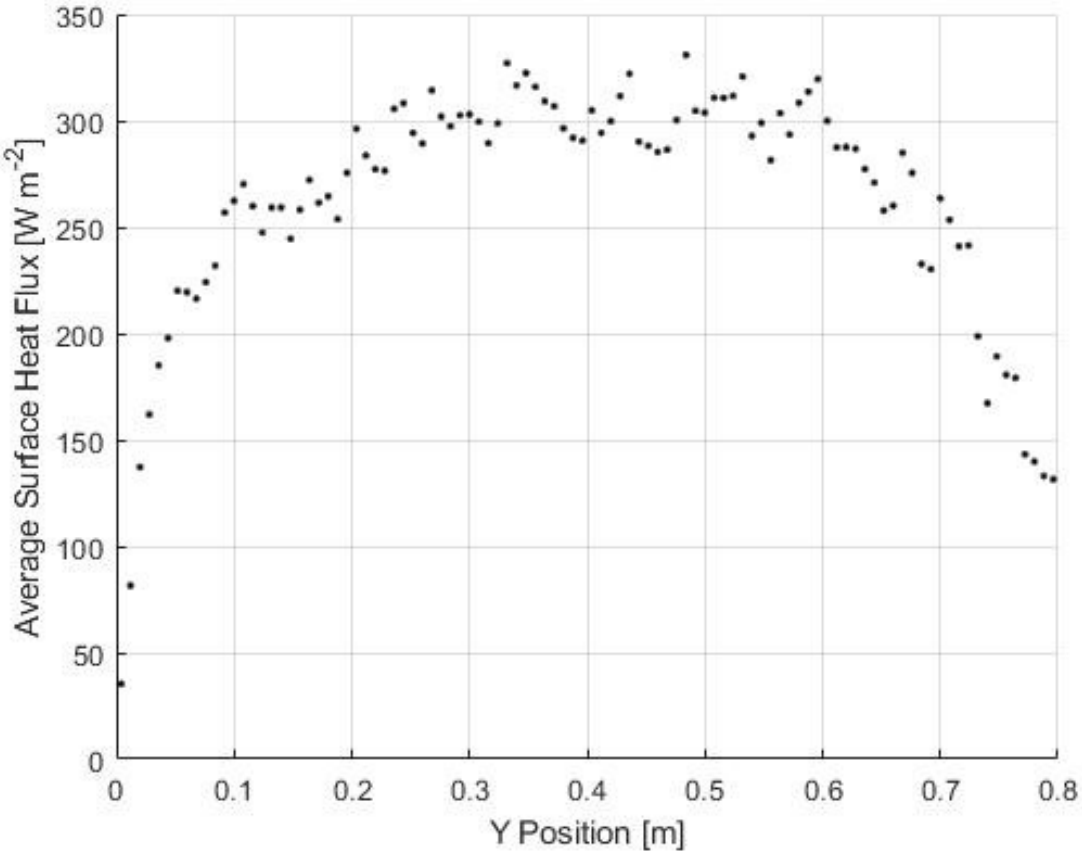

Figure 3: Average Surface Heat Flux as a function of Y Position

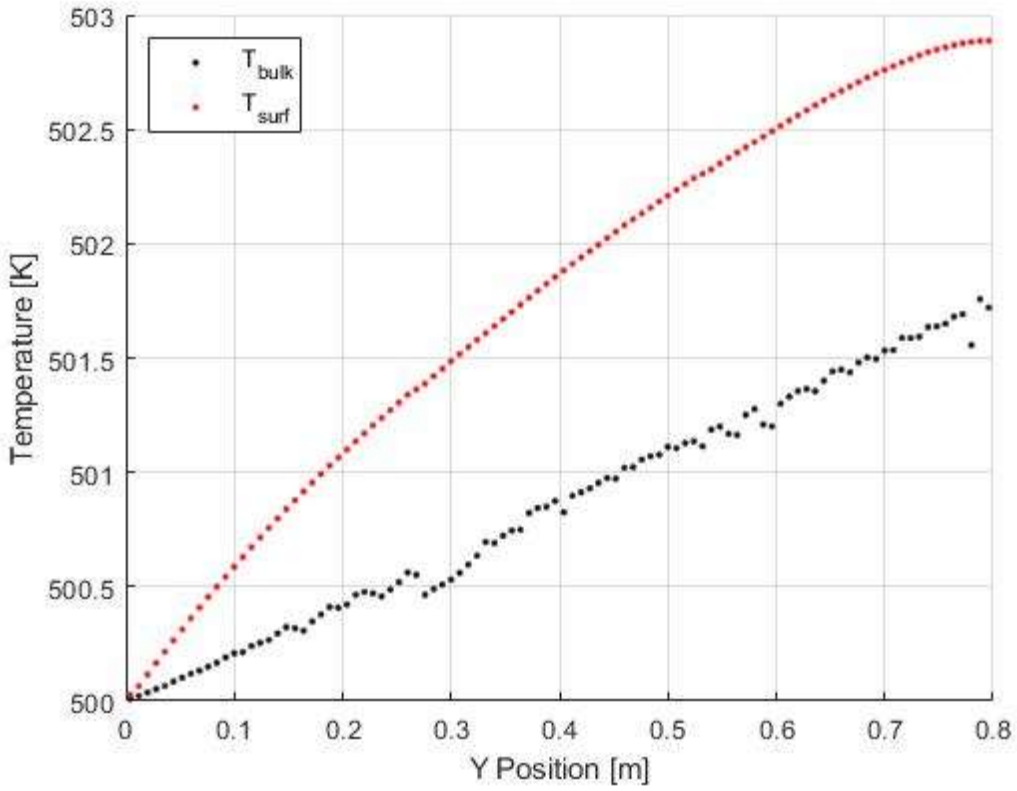

Figure 4: T_{bulk} and T_{surf} as a function of Y Position

Applying Equation 6 and Equation 7 to the values exported from Fluent, the Nusselt number as a function of height was calculated, and was shown in Figure 5. Similar to the cases investigated by Kays et al, the Nusselt number appears to approach infinity as position approaches zero, and as the flow develops it decays to an asymptotic value. This case does not appear to be fully developed, as the Nusselt number has not converged to a constant value. However, it should be noted that the Nusselt number of the flow as it reached the end of the domain was equal to 3.397 and still decreasing. This value was lower than either of the values for the constant wall temperature and constant heat flux cases proven by Kays et al. which was likely due to the internal heat generation of the fluid, leading to a less effective heat removal capability and thus reducing the magnitude of the convective heat transfer coefficient. The local heat transfer coefficient as a

function of y position was plotted in Figure 6, and as expected for developing flow exhibited the local maximum at the beginning of the domain and decreased in magnitude as it traversed the flow path. The channel average value of heat transfer coefficient was 409.544 W m^{-2} K^{-1}.

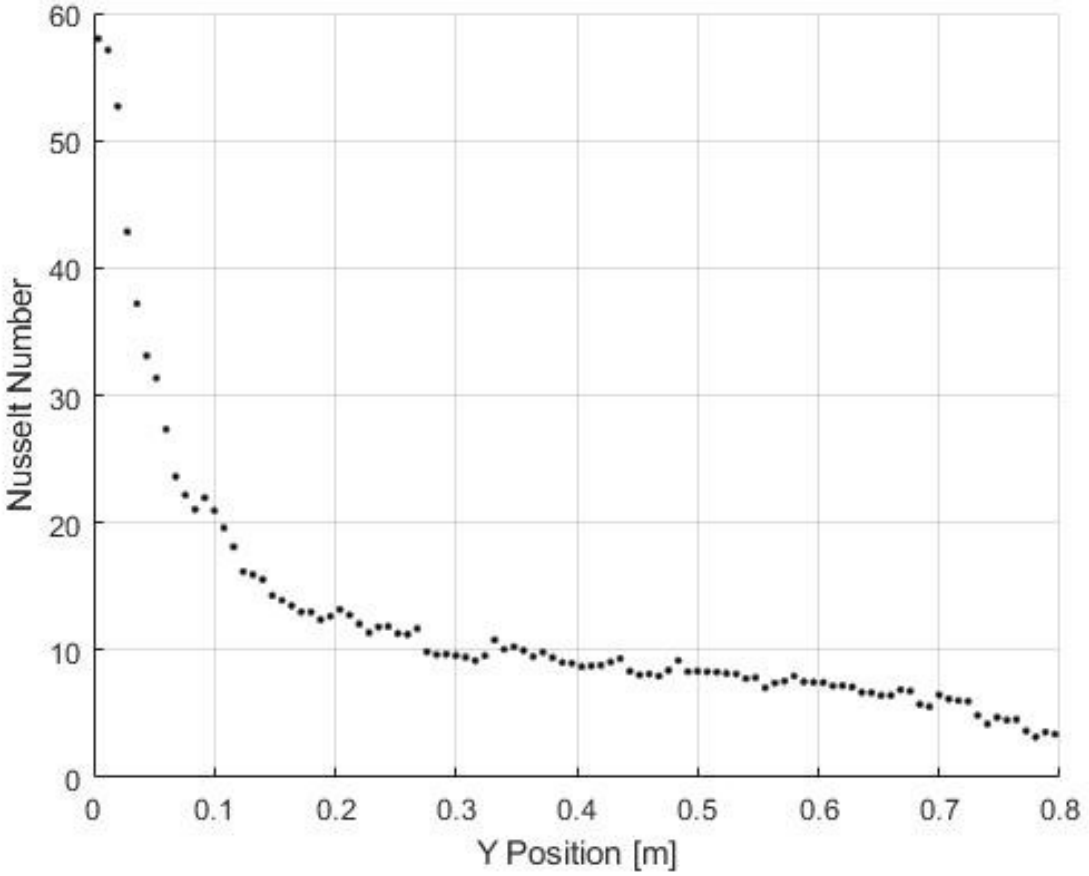

Figure 5: Nusselt Number as a function of Y Position

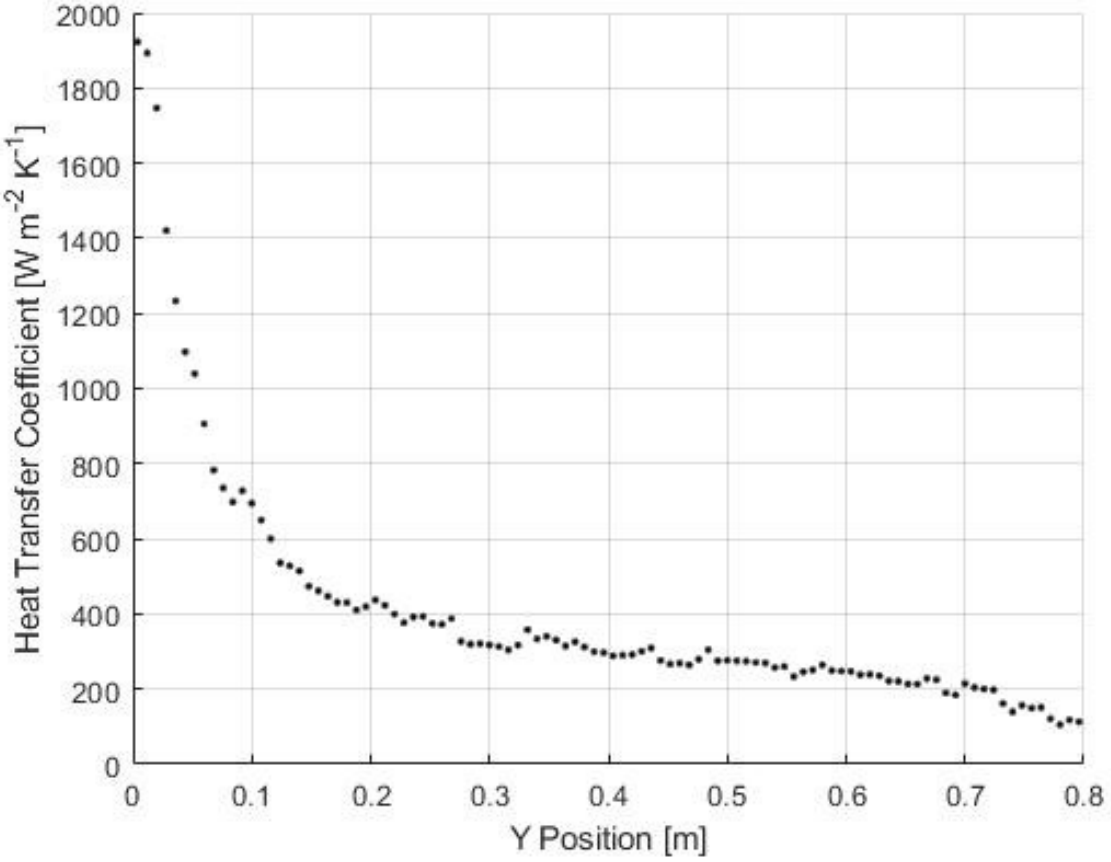

Figure 6: Average Heat Transfer Coefficient as a function of Y Position

Core Wedge Results

The identification of the ideal mass flow rate distribution in the core wedge was carried out by distributing the mass flow rate across each channel, and parametrically investigating until an optimal case was found. Specifics upon how the mass flow rate was distributed, as well as the parameters of interest which each case will be evaluated on are discussed in this section. The optimal case then had its fuel channel at the center of the computational domain, that is the radial midpoint, evaluated to characterize the combined entry length behavior of the fuel salt as it traverses the computational domain.

Mass Flow Distribution

From a top-down view of the core wedge, as shown in Figure 7, it was apparent that there are four rings of channels about the central axis. To efficiently parameterize the maximum temperature and the thermal gradient as a function of flow distribution, each ring was assessed a percentage of the total mass flow rate (1.6667 kg s^{-1}), with each ring having a uniform velocity at the inlet of each channel. The case matrix was shown in Table 4, and visually represented in Figure 8. More complete case matrices which describe the same set of simulations but also provide the associated velocity imposed upon each channel in that ring as well as the tabulated mass flow for each channel in each case are included within the APPENDIX. It should be noted that Case 13 represents an iso-velocity distribution, where all channels have identical velocities imposed at the inlet, thus the mass flow distribution in each ring was completely dependent upon the total fluid cross-sectional area in that ring.

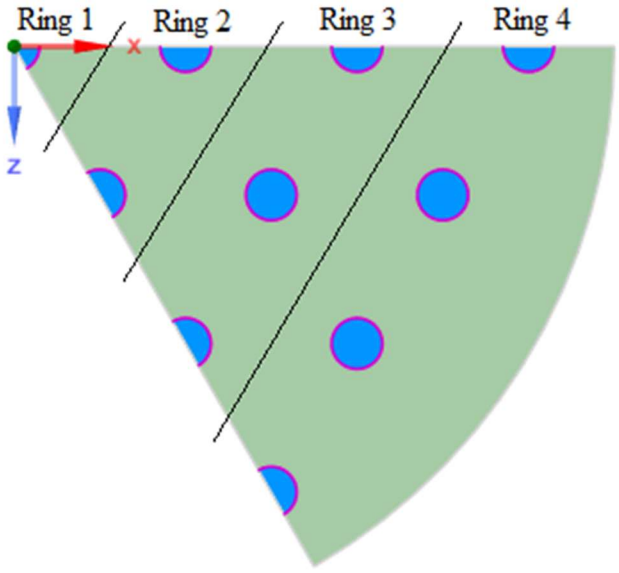

Figure 7: Top-down View of Core Wedge

Table 4: Core Wedge Case Matrix

Case #	Ring 1 ṁ %	Ring 2 ṁ %	Ring 3 ṁ %	Ring 4 ṁ %	Max Temperature [K]	Uniformity Index
Case 1	5.00%	20.00%	35.00%	40.00%	514.409	0.99906
Case 2	10.00%	20.00%	30.00%	40.00%	516.325	0.99906
Case 3	15.00%	20.00%	40.00%	25.00%	512.719	0.99911
Case 4	25.00%	25.00%	25.00%	25.00%	519.418	0.99862
Case 5	30.00%	25.00%	25.00%	20.00%	521.123	0.99835
Case 6	35.00%	35.00%	20.00%	10.00%	534.890	0.99676
Case 7	40.00%	30.00%	20.00%	10.00%	535.102	0.99679
Case 8	50.00%	16.67%	16.67%	16.67%	527.858	0.99803
Case 9	50.00%	20.00%	20.00%	10.00%	535.313	0.99691
Case 10	60.00%	13.33%	13.33%	13.33%	533.968	0.99762
Case 11	70.00%	10.00%	10.00%	10.00%	543.447	0.99702
Case 12	80.00%	10.00%	5.00%	5.00%	572.667	0.99476
Case 13	2.70%	16.22%	32.43%	48.65%	518.305	0.99878

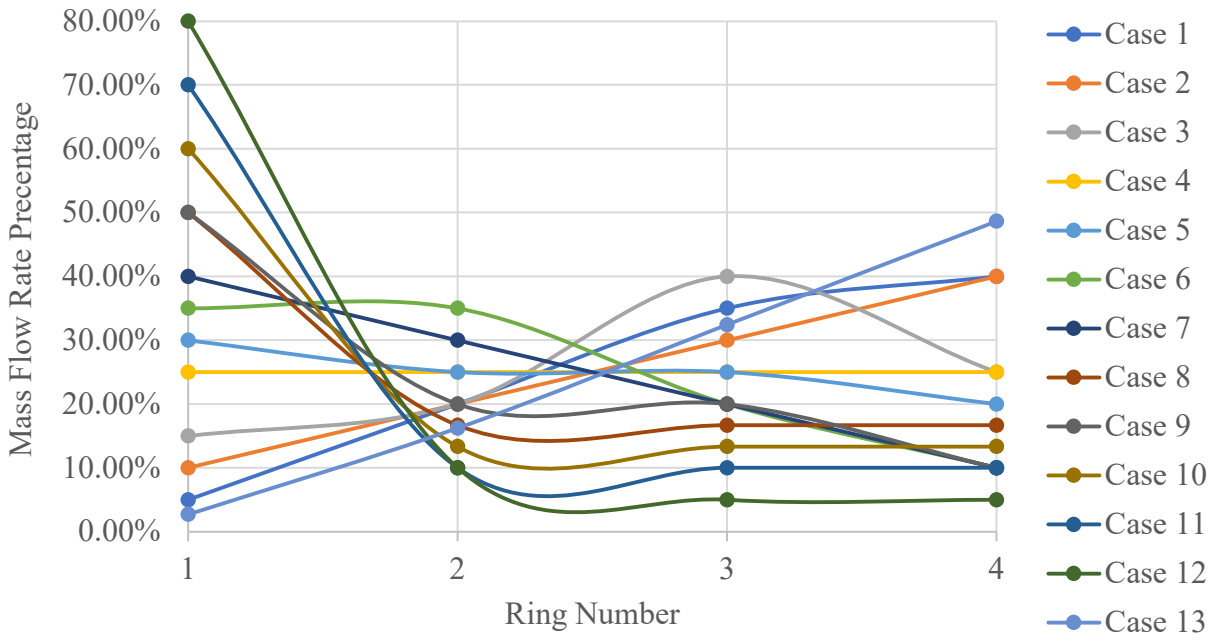

Figure 8: Mass Flow Distribution, Case Matrix

The first case ran was Case 4, as it represented an even amount of mass flow distribution to each ring. Utilizing the contour feature in Fluent, a visual representation of the temperature in the fluid and solid domains was generated, shown in Figure 9, and visually evaluated to inform as to how further cases should be designed. The maximum temperature was in the graphite as hypothesized, specifically in the outer core region comprised of rings 3 and 4. Despite the graphite's heat generation profile being of higher magnitude in the center of the core, the bulk of the graphite's mass was located in the outer region. As such the higher mass of graphite requires more coolant than the central region of the core.

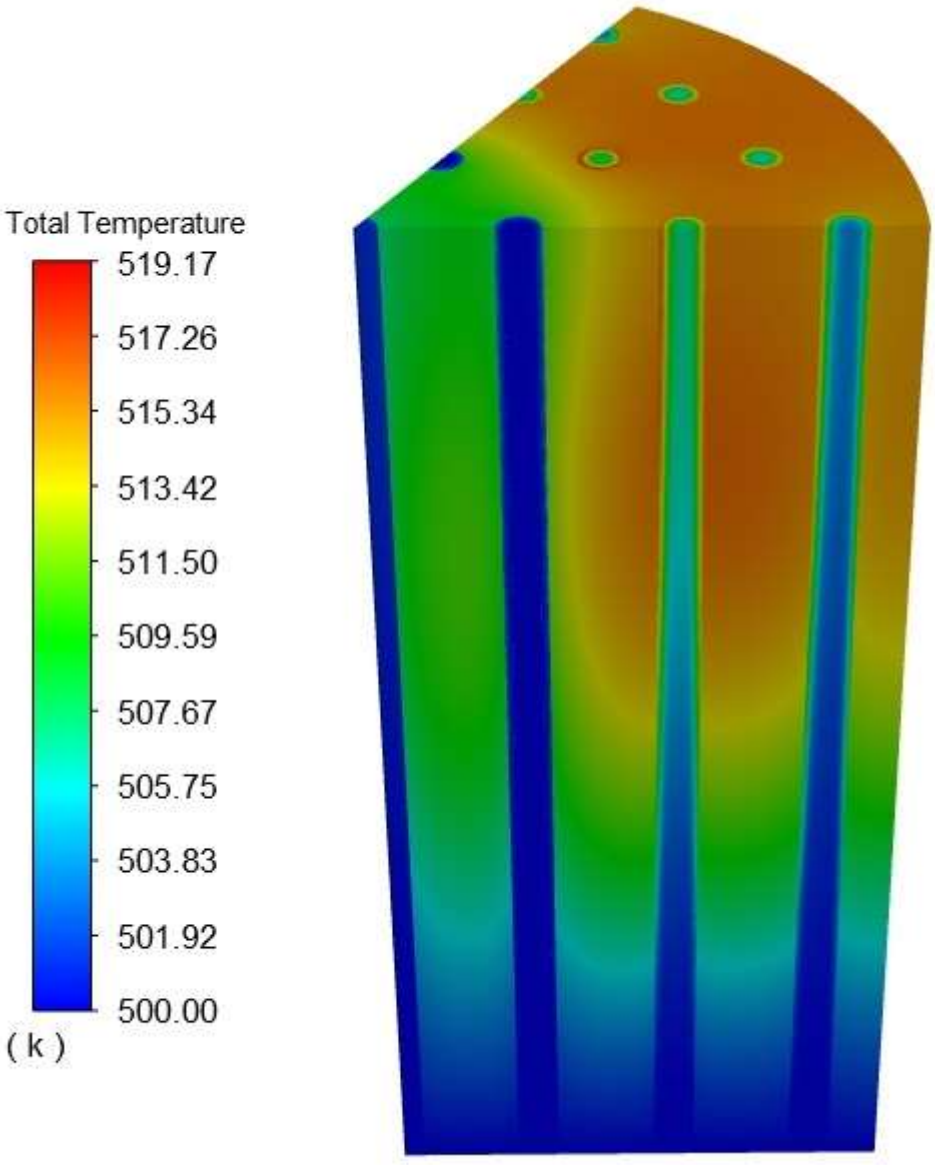

Figure 9: Contour of Case 4, Temperature

To relate the mass flow distribution to the parameters of interest, that is maximum temperature and temperature gradient in the radial direction, the flow distribution was reduced to a singular value which the parameters of interest we plotted against. The reduced value was the sum of the mass flow rate percentages in rings 3 and 4, as this represents the percentage of flow in

the outer region of the core model and was referred to as ṁ-34. Maximum temperature is plotted as a function of ṁ-34 in Figure 10, and it was clearly evident that there is an inverse trend exhibited up to 60 %, after which the data appears to become independent of ṁ-34. Figure 11 showed the uniformity index as a function of ṁ-34, which exhibited a direct relationship with ṁ-34 again up to the 60 % mark, and then appears to be independent of ṁ-34. From Figure 10 and Figure 11, it was clearly evident that more mass flow rate being distributed to the outer region leads to more desirable results for thermal management.

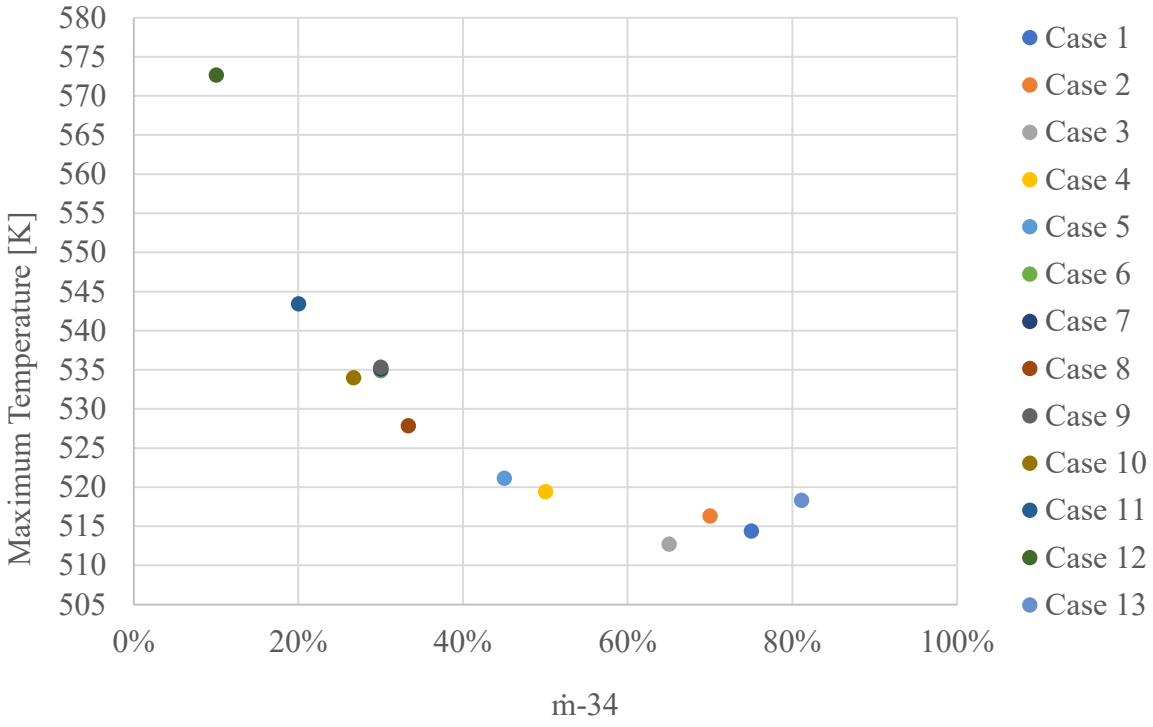

Figure 10: Maximum Temperature as a function of ṁ-34

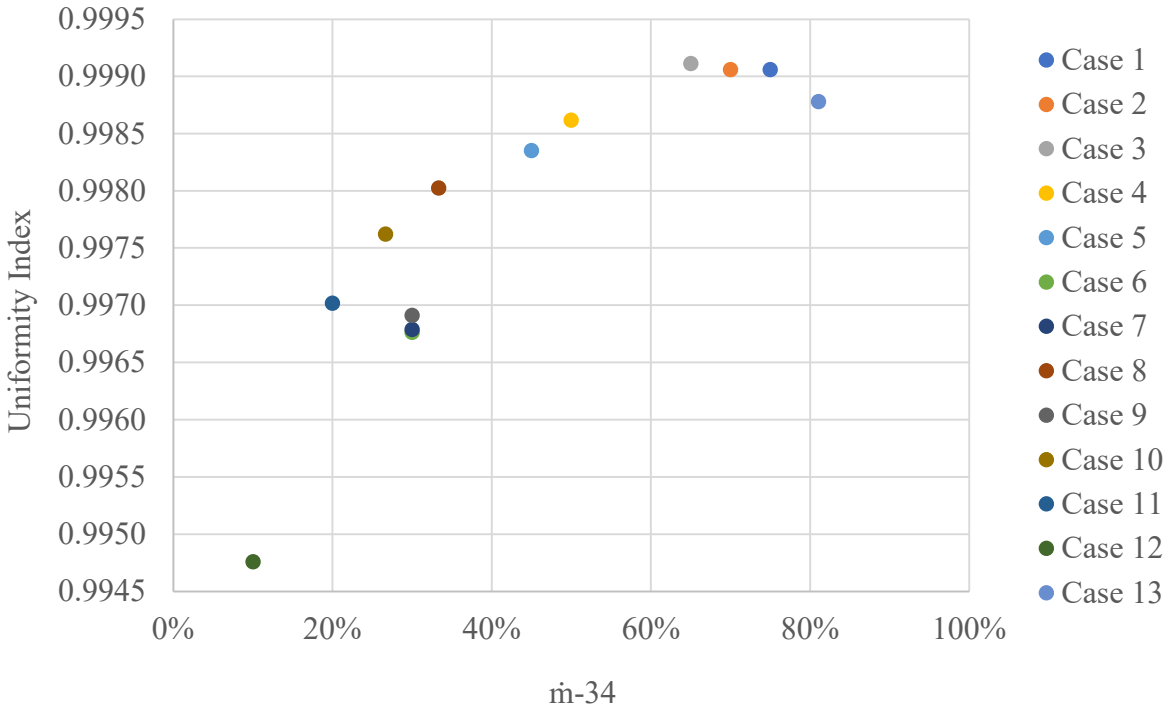

Figure 11: Uniformity Index as a function of ṁ-34

From a purely physics standpoint, it stands to reason that the case with the lowest maximum temperature would have the highest index of uniformity and therefore smallest thermal gradient. Whereas the case with the largest thermal gradient, represented as the index of uniformity would exhibit a larger range of temperatures within the domain, allowing for a higher maximum temperature. This is graphically shown in Figure 12, where the maximum temperature is plotted as a function of the index of uniformity for each case, and it is clearly evident that as the index of uniformity approaches 1, the maximum temperatures decrease in the domain. It is clearly evident that the best-found case for flow distribution based upon the parameters of interest was Case 3, as it exhibited the lowest maximum temperature and had the highest index of uniformity.

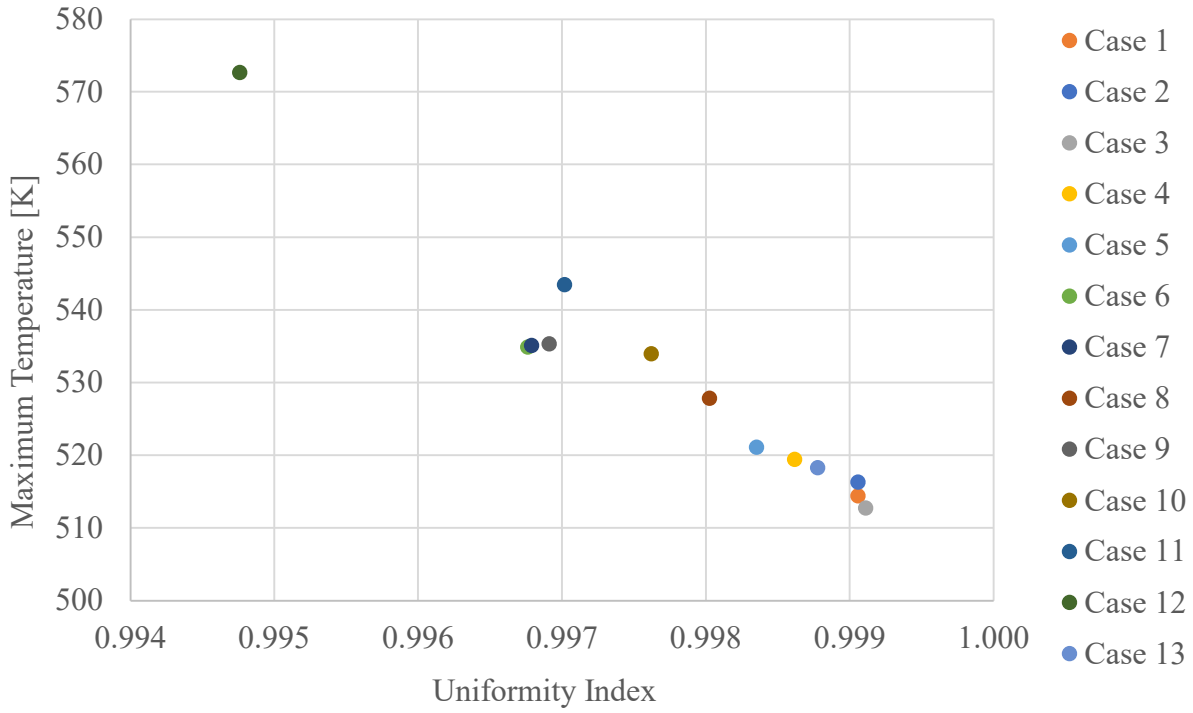

Figure 12: Maximum Temperature as a function of Uniformity Index

Non-Dimensional Temperature Increase

To quantify the effect of non-optimal flow distribution, a non-dimensional temperature rise was calculated using Equation 8. This theta value quantifies the maximum temperature in relation to the average temperature increase expected, which can be calculated if the heat generation profile is known. The results of applying this equation to each case are shown below in Table 5. Case 3 had the minimum theta value of 1.272, with Case 12 having the maximum value of 7.267. A value of 7.267 represents a maximum temperature in the domain that is 7.267x the expected temperature increase of the coolant across the core, which is excessively high. If the core was operating on a power level that would increase the coolant by 25 Kelvin, with the non-optimal flow distribution the maximum temperature could reach as high as 180 Kelvin above the average outlet temperature.

However, with the optimal flow distribution, the maximum temperature would only reach approximately 30 Kelvin above the average outlet temperature. This quantification of the non-optimal flow distribution is paramount when assessing how the flow should be distributed in a molten salt reactor core, as it informs to the adverse effects of non-optimal design.

Equation 8: Non-Dimensional Temperature Increase

$$\theta = \frac{T_{max} - T_{inlet}}{T_{outlet} - T_{inlet}}$$

Where,

θ is the non-dimensional temperature increase

T_{max} is the maximum temperature in the domain in Kelvin

T_{inlet} is the inlet temperature to the domain in Kelvin

T_{outlet} is the average outlet temperature of the fuel salt, in Kelvin

Table 5: Tabulated Values of Non-Dimensional Temperature Increase

Case #	ṁ-34	Max Temperature [K]	Theta θ
Case 1	75.00%	514.409	1.441
Case 2	70.00%	516.325	1.633
Case 3	65.00%	512.719	1.272
Case 4	50.00%	519.418	1.942
Case 5	45.00%	521.123	2.112
Case 6	30.00%	534.890	3.489
Case 7	30.00%	535.102	3.510
Case 8	33.33%	527.858	2.786
Case 9	30.00%	535.313	3.531
Case 10	26.66%	533.968	3.397
Case 11	20.00%	543.447	4.345
Case 12	10.00%	572.667	7.267
Case 13	81.08%	518.305	1.830

Combined Entry Length Behavior

To better understand Case 3, the radial midpoint fuel channel in the wedge had its entry length behavior evaluated in the same manner as the hexagonal unit cell. Solution data was exported from Fluent and loaded into a MATLAB script and evaluated to calculate the Nusselt number as a function of height within the simplified core. The results of this evaluation are shown in Figure 13 and Figure 14, where the combined entry length behavior mimics the thermal entry behavior exhibited by the hexagonal unit cell. The Nusselt number once again was large at the inlet to the channel and decayed down towards an asymptotic value, though the computational domain was not sufficiently long for the value to converge. This behavior could also be seen in the behavior of the heat transfer coefficient as a function of y position as shown in Figure 14. The channel average heat transfer coefficient was calculated to be 952.594 W m^{-2} K^{-1}, though it should

be noted that this average did not include the first three values in the computational domain as it heavily skewed the average due to them being on the order of 10^5 W m^{-2} K^{-1}. The oscillatory behavior of the Nusselt number indicated periodic thermally developing flow, where the Nusselt number decayed with oscillatory behavior. This behavior was likely due to the non-homogeneity of the heat generation profile in the domain.

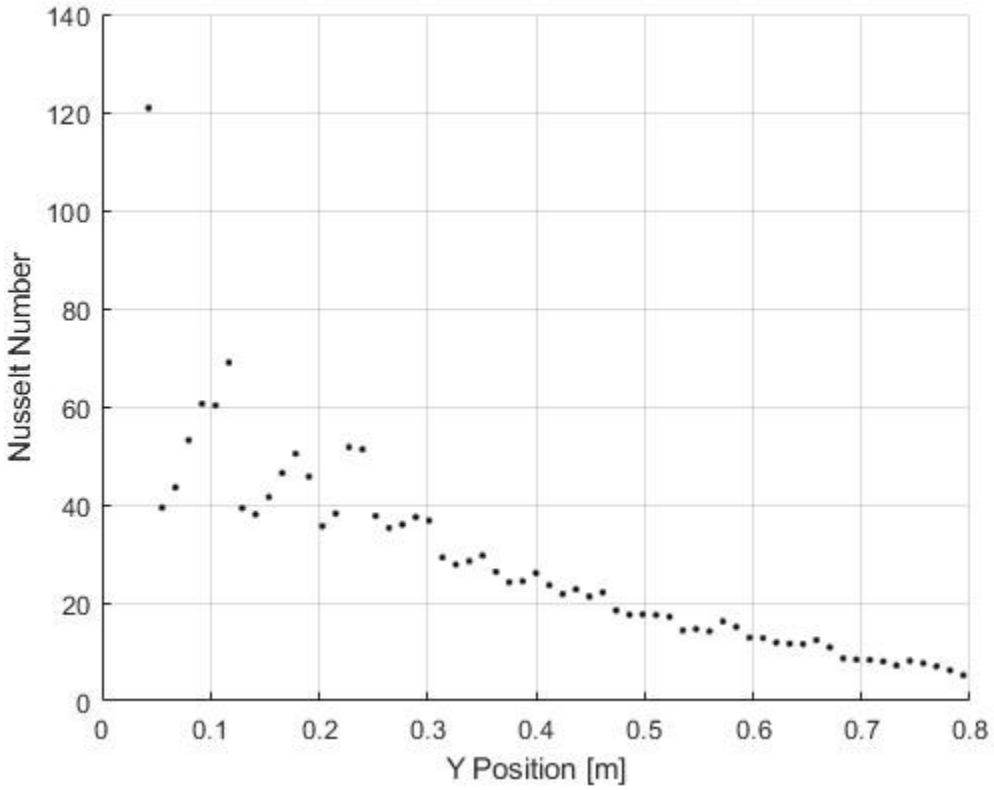

Figure 13: Nusselt Number as a function of Y Position, Case 3

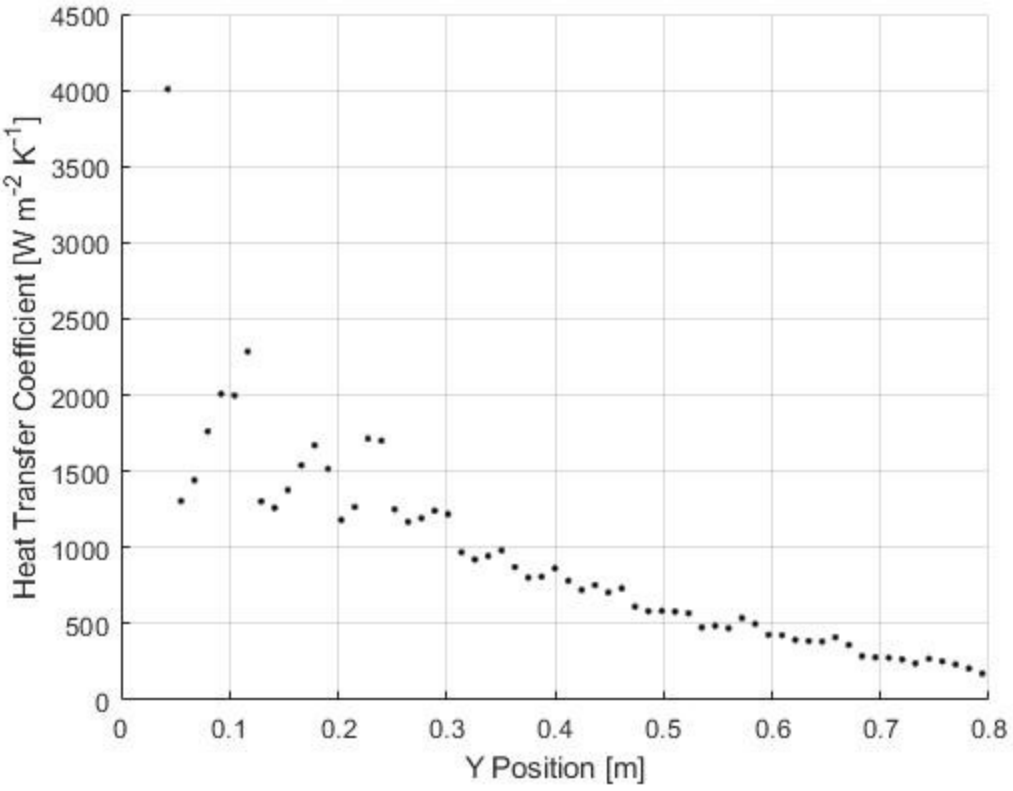

Figure 14: Heat Transfer Coefficient as a function of Y Position, Case 3

CONCLUSION

An investigation utilizing CFD to investigate thermal entry length behavior in a hexagonal unit cell, as well as the idealized mass flow distribution and the combined entry length behavior was carried out. Thermal entry length behavior was a novel investigation due to the presence of heat generation in the fluid as well as the solid regions of the domain, as such the thermal boundary condition upon the wall was neither constant heat flux nor temperature. It was found that Nusselt number decayed below the converged Nusselt number for the before mentioned thermal boundary conditions and had not yet converged when the computation domain ended. This is likely due to the presence of internal heat generation in the fluid reducing the fluid's ability to remove heat, as the temperature of the fluid is constantly increasing due to both the convective heat flux from the wall as well as the internal heat generation source term. A simplified model of a liquid-fuel molten salt reactor was created by arranging the hexagonal unit cell into a circular array and then slicing into a 60-degree wedge to reduce the required computational resources. Internal heat generation in both the fluid and solid domains was implemented that was both radially and axially dependent to replicate the power generation profiles that occur in typically power reactors. To identify the best-case distribution of mass flow rate, the maximum temperature and thermal gradient were evaluated for each case. The optimal case found was Case 3, which had a 15-20-40-25 % split through the 4 annular sections of the simplified core model. This split limited the maximum temperature in the computational domain to 512.719 K and reached a thermal uniformity index of 0.99 in the axial midplane. A non-dimensional temperature increase was proposed and evaluated for each case on the core wedge domain to quantify the effect of non-optimal flow distribution in regards to maximum temperature. It was found that the optimal flow distribution had a non-dimensional temperature increase (theta) value of 1.272, and for the least optimal case theta

reached 7.267. The theta value allows for an estimation of maximum temperature in the domain based upon the inlet and average outlet conditions, which can be calculated if the power distribution is known. This value informs to the adverse effects of non-optimal flow distribution and allows for designers to evaluate the maximum temperature in the domain based upon flow distribution and operating power. The central channel of Case 3 (optimal case) was evaluated in the same manner as the hexagonal unit cell, where periodic thermally developing flow behavior was exhibited in the channel as indicated by oscillatory decay behavior. The Nusselt number in the channel did not fully-develop in the computational domain but did decay below the values for constant heat flux and constant temperature wall boundary conditions.

Future Works

While this investigation provided key insight towards the nature of the developing flows that occur in a liquid-fuel molten salt reactor, it was in no-way all encompassing. The author has identified the following 5 areas for future work should be carried out to better characterize the thermal-hydraulic behavior in a molten salt reactor.

Firstly, the hexagonal unit cell domain simulation should be rerun with a larger flow domain, allowing for the flow to fully develop to evaluate what the converged Nusselt number would be for flows of this nature. Second, implementation of nuclear fuel salt thermophysical properties, rather than those of non-nuclear fuel salts, should be carried out when a specific enrichment and mixture percentage are known for a desired reactor design. As the results of a thermal-hydraulic investigation rely heavily upon the thermophysical properties of the fluid, it should be expected that the ideal mass flow distribution will change with a different coolant salt. Third, thermophysical properties were all considered to be constant, which may not be the best

representation of real-world physics. When the nuclear fuel salt data is known the temperature dependence of thermophysical properties should be implemented. Fourth, a transient simulation of the core wedge should be carried out to ensure that in the approach to steady state there are no regions that undergo excessive heating before the coolant can remove the thermal energy. Fifth, a dynamic mesh that can properly model the thermal expansion of the graphite should be carried out to ensure that the thermal gradient and subsequent variation of density in the graphite does not inhibit the ability of the coolant to keep all regions of the graphite below the thermal limitations.

REFERENCES

1. Generation IV International Forum “Annual Report 2021”, December 2021
2. F. P. Incropera and D. P. Dewitt, “Fundamentals of heat and mass transfer,” 4th Edition, John Wiley and Sons, Hoboken, 1996.
3. Stacey, Weston M. *Nuclear Reactor Physics*. Wiley-VCH, 2018.
4. “Part 50-Domestic Licensing of Production and Utilization Facilities.” NRC Web, https://www.nrc.gov/reading-rm/doc-collections/cfr/part050/full-text.html#part050-0036.
5. Rosenthal, M. W., P. R. Kasten, and R. B. Briggs. "Molten-salt reactors—history, status, and potential." Nuclear Applications and Technology 8.2 (1970): 107-117.
6. Haubenreich, Paul N., and J. R. Engel. "Experience with the molten-salt reactor experiment." Nuclear Applications and technology 8.2 (1970): 118-136.
7. Beall, S. E., et al. Msre design and operations report. part v. reactor safety analysis report. No. ORNL-TM-732. Oak Ridge National Lab., Tenn., 1964.
8. “NEXT Collaboration.” *NEXTRA,* www.acunextlab.org/nextra
9. Kays, W.M., and M.E. Crawford, *Convective Heat and Mass Transfer*, McGraw-Hill, New York, 1980
10. ANSYS, Inc. "ANSYS Meshing User’s Guide Release 15.0." (2013).
11. Sohal M.S., Ebner M.A, Sabharwall P., Sharpe P. “Engineering Database of Liquid Salt Thermophysical and Thermochemical Properties” *Idaho National Labs Digital Library*, INL June 2013, pg 14
12. Magnusson, Jared, Matthew Memmott, and Troy Munro. "Review of thermophysical property methods applied to fueled and un-fueled molten salts." Annals of Nuclear Energy 146 (2020): 107608.

13. McEligot, Donald, Swank, W. David, Cottle, David L., and Valentin, Francisco I.. Thermal Properties of G-348 Graphite. United States: N. p., 2016. Web. doi:10.2172/1330693.
14. ANSYS, Inc. "ANSYS Fluent User's Guide Release 15.0." (2013).
15. Lewis, Elmer E. Fundamentals of nuclear reactor physics. Elsevier, 2008.
16. Todreas, Neil E., and Mujid S. Kazimi. Nuclear systems volume I: Thermal hydraulic fundamentals. CRC press, 2021.
17. ANSYS, Inc. "ANSYS Fluent Theory Guide Release 15.0." (2013).

APPENDIX

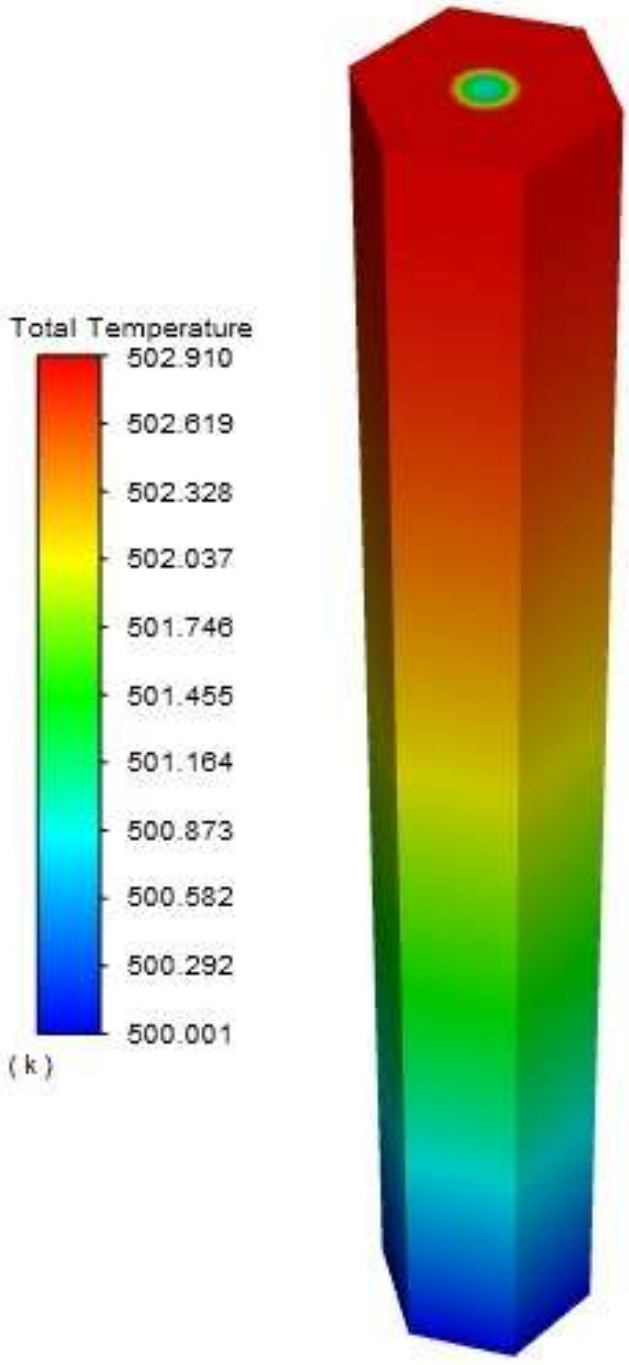

Figure 15: Contour of Total Temperature, Hexagonal Unit Cell

Table 6: Full Case Matrix, Core Wedge

Case #	Ring 1 Mass Flow %	Ring 1 Velocity [m/s]	Ring 2 Mass Flow %	Ring 2 Velocity [m/s]	Ring 3 Mass Flow %	Ring 3 Velocity [m/s]	Ring 4 Mass Flow %	Ring 4 Velocity [m/s]	Maximum Temperature [K]	Uniformity Index
Case 1	5.0%	0.361	20.0%	0.241	35.0%	0.210	40.0%	0.160	514.409	0.99906
Case 2	10.0%	0.722	20.0%	0.241	30.0%	0.180	40.0%	0.160	516.325	0.99906
Case 3	15.0%	1.082	20.0%	0.241	40.0%	0.241	25.0%	0.100	512.719	0.99911
Case 4	25.0%	1.804	25.0%	0.301	25.0%	0.150	25.0%	0.100	519.418	0.99862
Case 5	30.0%	2.165	25.0%	0.301	25.0%	0.150	20.0%	0.080	521.123	0.99835
Case 6	35.0%	2.525	35.0%	0.421	20.0%	0.120	10.0%	0.040	534.890	0.99676
Case 7	40.0%	2.886	30.0%	0.361	20.0%	0.120	10.0%	0.040	535.102	0.99679
Case 8	50.0%	3.608	16.7%	0.200	16.7%	0.100	16.7%	0.067	527.858	0.99803
Case 9	50.0%	3.608	20.0%	0.241	20.0%	0.120	10.0%	0.040	535.313	0.99691
Case 10	60.0%	4.329	13.3%	0.160	13.3%	0.080	13.3%	0.053	533.968	0.99762
Case 11	70.0%	5.051	10.0%	0.120	10.0%	0.060	10.0%	0.040	543.447	0.99702
Case 12	80.0%	5.772	10.0%	0.120	5.0%	0.030	5.0%	0.020	572.667	0.99476
Case 13	2.7%	0.195	16.2%	0.195	32.4%	0.195	48.6%	0.195	518.305	0.99878

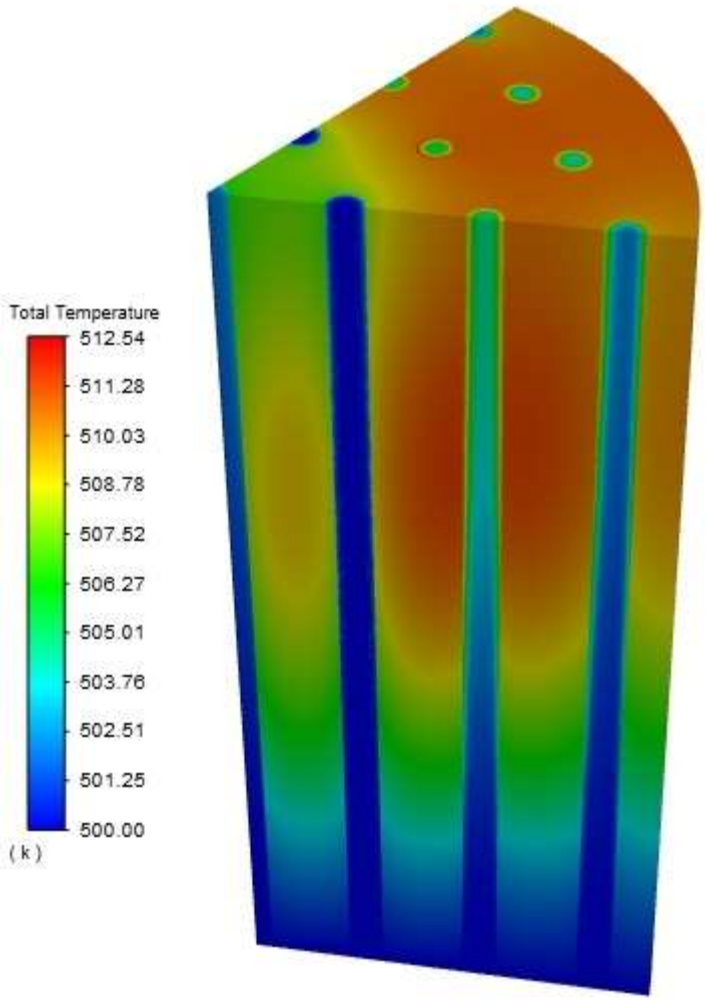

Figure 16: Contour of Total Temperature, Core Wedge Case 3

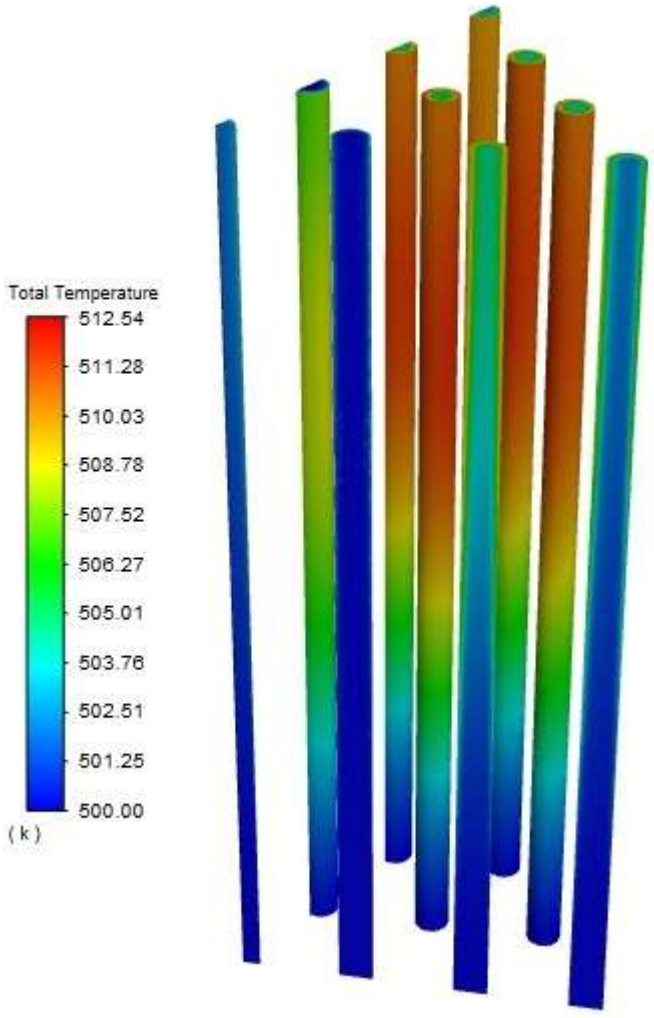

Figure 17: Contour of Total Temperature, Core Wedge Case 3 Fluid Only

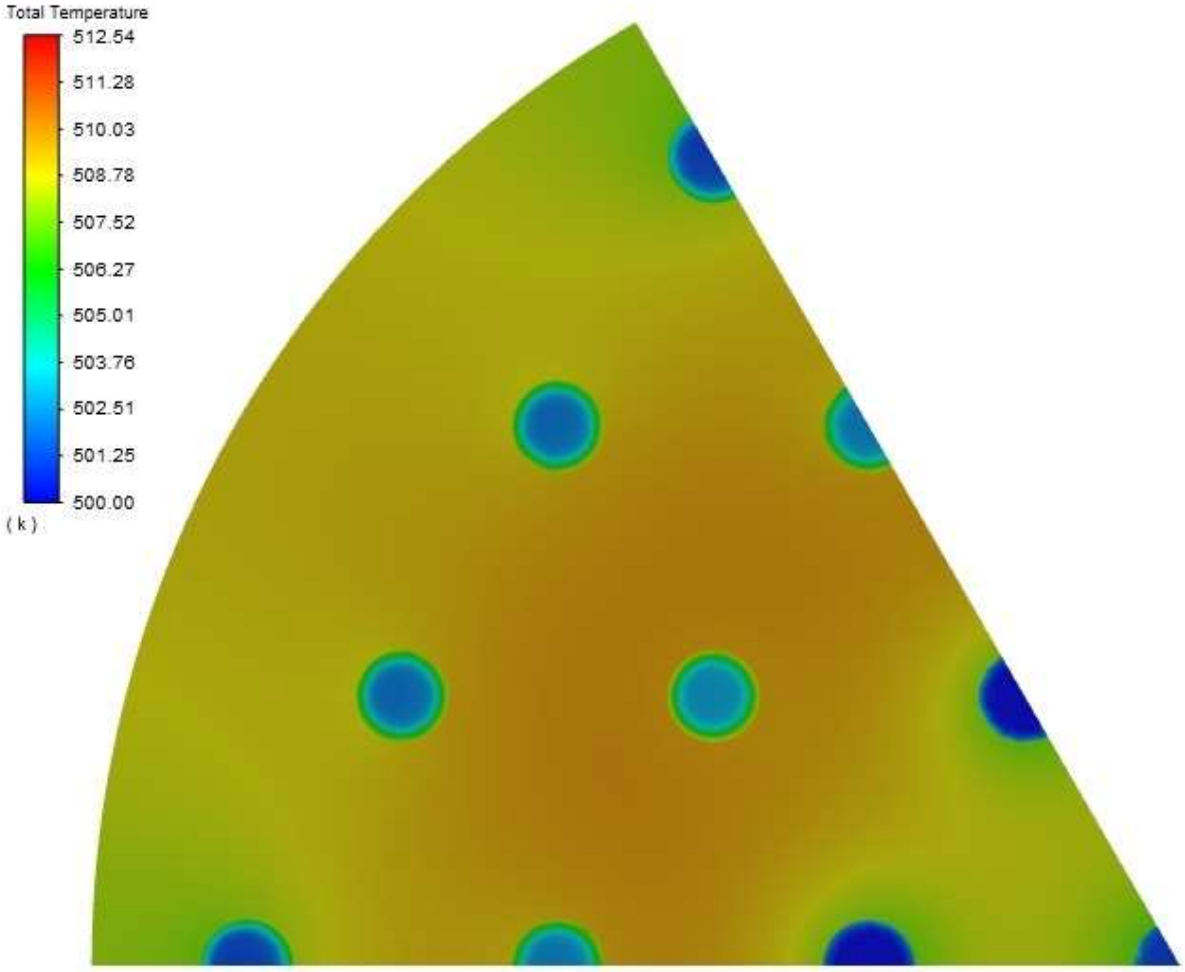

Figure 18: Contour of Total Temperature, Case 3 Axial Midplane

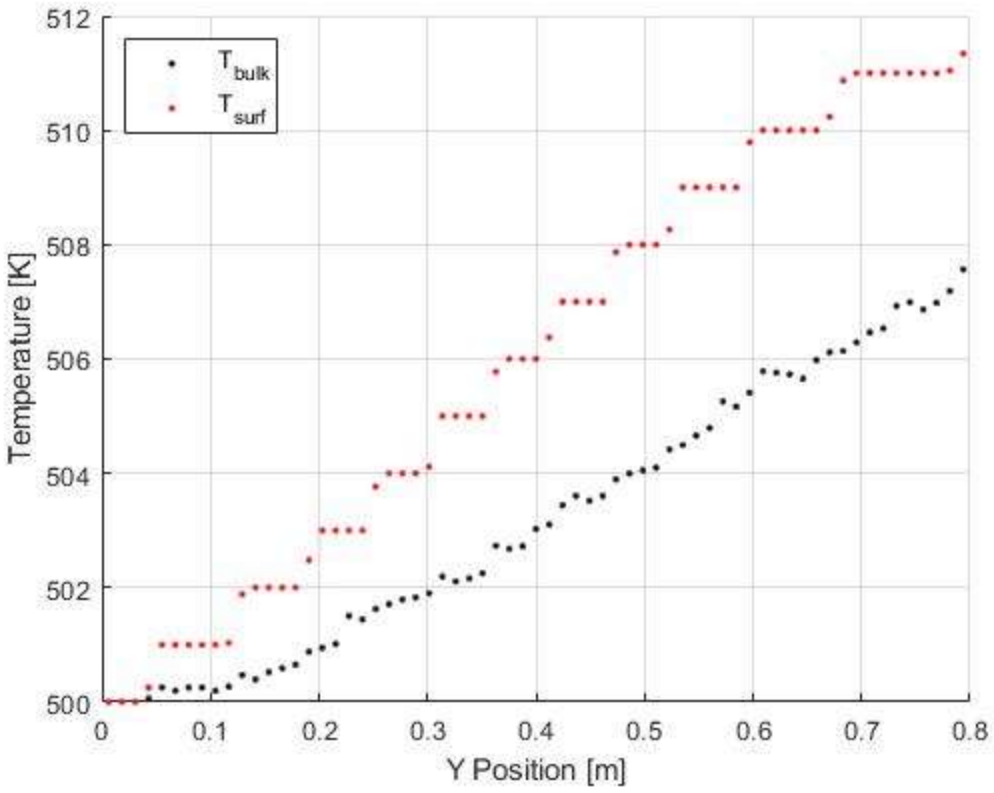

Figure 19: T_{bulk} and T_{surf} , Case 3 Radial Midpoint Channel

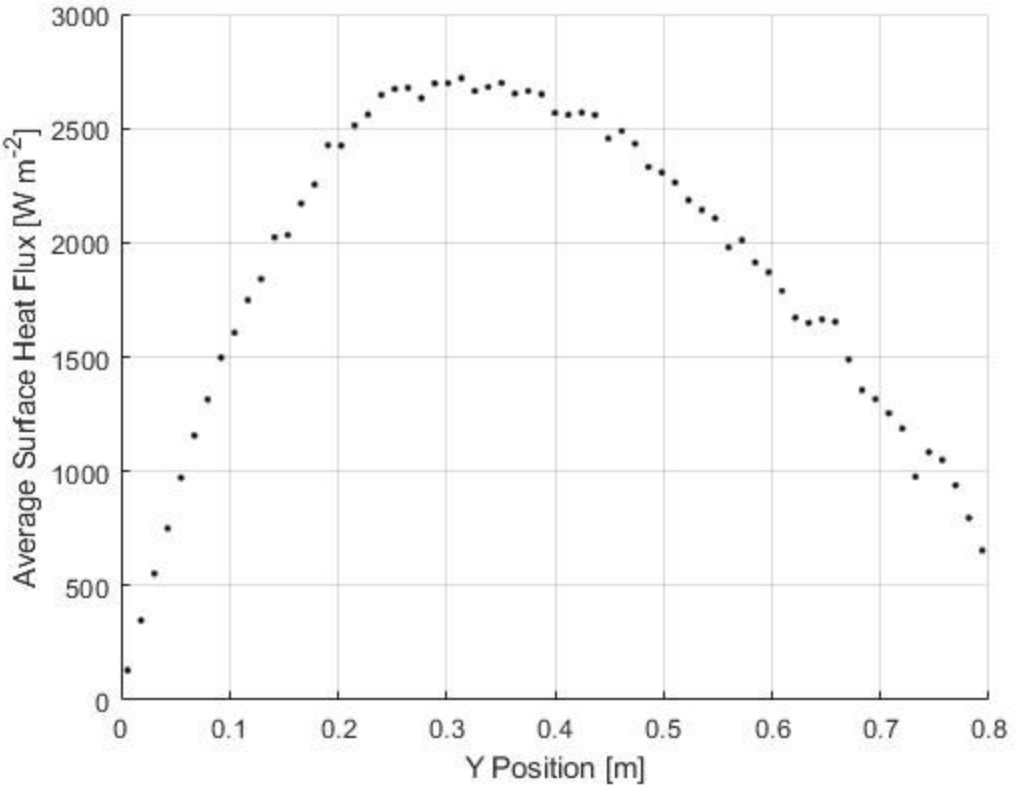

Figure 20: Average Surface Heat Flux as a function of Y Position, Core Wedge